The friction stir welding of small-diameter pipe: an experimental and numerical proof of concept for automation and manufacturing

D H Lammlein*, **B T Gibson, D R DeLapp, C Cox, A M Strauss,** and **G E Cook**
Welding Automation Lab, Vanderbilt University, Nashville, TN, USA

The manuscript was received on 3 August 2010 and was accepted after revision for publication on 14 February 2011.

DOI: 10.1177/0954405411402767

Abstract: Friction stir welding (FSW) is a powerful joining process which is limited by its range of application and processing rate. Here the range of application is extended to small-diameter butted pipe sections and high processing rates are applied for increased productivity in manufacturing. Full penetration friction stir welds are performed on butted sections of aluminium alloy 6061-T6 pipe. These pipe sections are relatively small in diameter (4.2 inches) and relatively thin walled (0.2 inches). The small radius of curvature distinguishes this weld configuration geometrically from a butted plate configuration and presents unique challenges. This work confronts these challenges using experimental and numerical methods. An FSW process method producing acceptable pipe joints is demonstrated.

Keywords: friction stir welding, butted pipes, butted cylinders, computational fluid dynamics

1 INTRODUCTION

Friction stir welding (FSW) is an effective and consistent materials joining technology which produces high-strength and high-integrity joints, particularly in aluminium alloys [**1**]. FSW is also attractive because it is a solid-state process, with temperatures not exceeding the melting point of the work material. Its use is limited primarily by the combined expense of the FSW machine itself and the lack of an operating knowledge base. However, superb joint quality and low continuing operating costs for the machine mean that this initial expense can often be justified, particularly in vehicular applications (aerospace, automotive, and rail). FSW has been demonstrated on standard geometries like butted, lapped, and T-oriented joints. Its implementation on small-diameter pipes could extend its use to the petroleum, petrochemical, and natural gas industries where high weld volume would justify the upfront costs of FSW.

Additionally, FSW at a high rate of traverse (or travel) would increase output for manufacturing and further reduce the energy expended per unit length of weld. High traverse rates are tested in this work with good results. By increasing the rate of traverse, the time spent by the work at elevated temperatures is reduced and the total heat input into the pipe sections is reduced. Excessive heat is undesirable, as it causes detrimental changes in the material properties of the parent material.

Fusion welds are performed commonly on small-diameter aluminium pipe [**2, 3**]. The high heat input and temperatures present in fusion welding are the primary drawback to this approach, particularly in small-diameter pipes. Groove type, gas shielded arc welding is the most common fusion welding method performed on aluminium alloy pipes. The primary drawback of this method is the high temperatures and heat input result in a softening of the surrounding base metal. In these welds the heat affected zone

*Corresponding author: Welding Automation Lab, Vanderbilt University, 2201 West End Ave Nashville, TN, USA, 37235.
email: david.h.lammlein@gmail.com

Downloaded from pib.sagepub.com at VANDERBILT UNIV LIBRARY on February 20, 2012

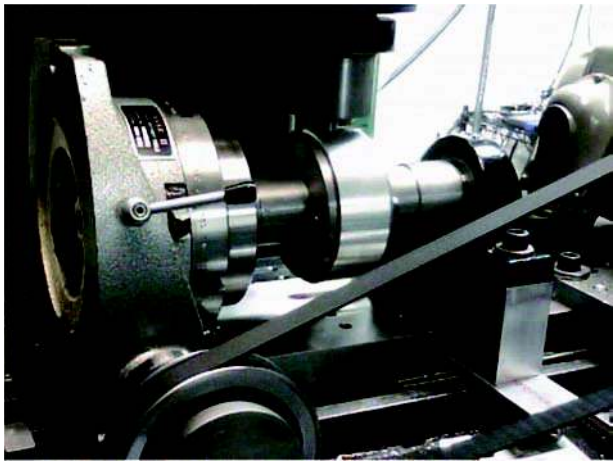

Fig. 1 The rotary welding apparatus used in this experiment is mounted to a standard FSW machine and rotates butted pipe sections below a stationary tool axis

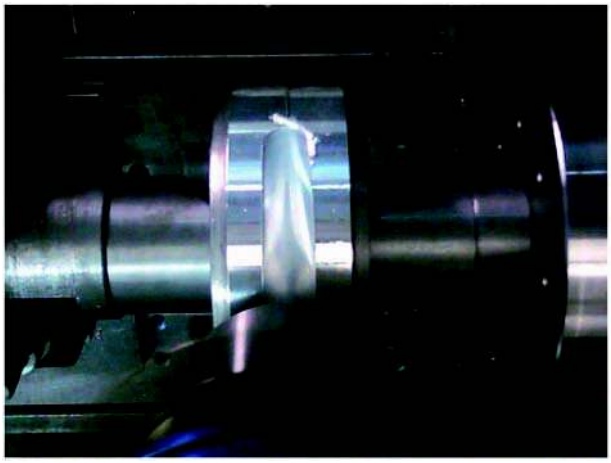

Fig. 2 A still image taken from video made during an experimental weld (top view)

(HAZ) controls the as-welded tensile strength of the joint in most cases [**4**]. This problem is exacerbated in small-diameter pipes and the reduced heat and solid-state nature of FSW makes it an attractive alternative in this application.

In this work, full-penetration friction stir welds are performed on butted sections of aluminium alloy 6061-T6 pipe. These pipe sections are relatively small in diameter (4.2") and relatively thin walled (0.2"). The small radius of curvature distinguishes this weld configuration geometrically from a butted plate configuration and presents unique challenges. These challenges necessitate the use of specialized techniques and specialized equipment. Friction stir welded joints of this type are not presented in academic literature, although FSW of large-diameter steel pipe sections is being done at a research level.

Collaboration between Advanced Metal Products Inc., Oak Ridge National Lab, and Megastir Technologies has produced an orbital welding apparatus for joining X65 steel [**5–7**]. The test device is designed to produce full-penetration welds on 12" diameter, 0.25" wall thickness pipe. This device revolves the tool about the stationary pipe and uses a hydraulic internal support fixture. Additionally, ExxonMobil has conducted research on FSW of line-pipe steels [**8**].

2 EXPERIMENTAL SETUP

In the present experiment, an experimental apparatus was designed, shown in Figs 1 and 2, which rotates the pipe sections beneath a stationary tool axis. The apparatus is mounted to an FSW machine and belt driven by a computer-controlled motor. The experimental apparatus has also been used by the authors to join small-diameter, butted Al-6061 hemispheres [**9**]. The internal support fixture, or mandrel, used in the present experiment serves an identical purpose to that used with the AMP/ORNL/Megastir orbital apparatus, but is of a different, manually actuated design.

The cylindrical work geometry presents a number of challenges that must be addressed. In addition to the obvious issue of tool geometry, the issues of secondary heating at the end of the weld, variation in the height of the work surface due to system eccentricity, the method of interior support, and the method of tool disengagement must be addressed. In this work, the significance of these issues are determined based on experimental and numerical results, and solutions are presented with applications to manufacturing. Disengagement, which can be achieved via an auto-adjustable probe tool as per Ding and Oelgoetz [**10**], the tapered retraction of a variable penetration conical tool as per Trapp and Fisher [**11**], or by a plug type method as per Takeshita and Hibbard [**12**], is not discussed in this work

It is apparent that the contact condition between a traditional, flat shoulder tool and small-diameter cylindrical work differs significantly from that of butted plate welding. Figure 3 shows an experimental tool used in the experiment over butted, cylindrical work samples prior to joining. The flat, circular shoulder does not sit flush with the work surface and, at a reasonable plunge depth, the shoulder must hang over the front of the cylinder, over the back of the cylinder, or both depending on the

Downloaded from pib.sagepub.com at VANDERBILT UNIV LIBRARY on February 20, 2012

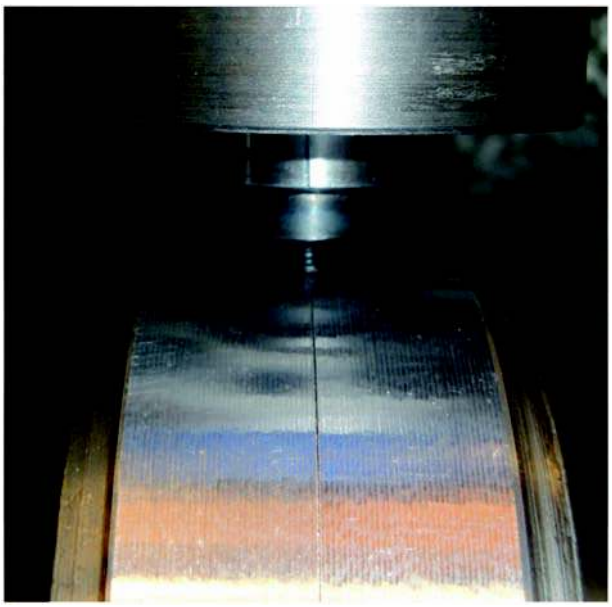

Fig. 3 A close-up view of a tool used in the experiment and the butted weld specimens used in the experiment. The pipe sections are shown mounted in the welding apparatus. The experiment is started from this position. The tool probe was position was calibrated, or zeroed, against the surface of the work. The tool rotation is started and the probe is plunged into the material until the desired contact is achieved with the shoulder on the cylindrical surface of the work

tool's offset from the work axis of rotation. This creates potential problems for the shoulder in its material containment role. It must be demonstrated experimentally that this issue is not significant in pipe welding if a traditional shoulder is to be used. In the current work, the tool is offset 6.0 mm forward of the work to create the ploughing effect common in FSW. This effect means the trailing edge of the shoulder is the portion deepest in the work. This ploughing effect is achieved on flat work by tilting the tool and creating a so-called angle of attack. The method presented in this work results in a similar contact condition and acceptable results.

The circular nature of the weld path in a butted pipe configuration results in a secondary heating at the end of the weld. To complete a full, circumferential weld, the tool must cross over the weld initiation site which remains warm for a small-diameter pipe. This additional heat affects the steady state portion of the weld and the weld termination. The highly coupled nature of the thermal and mechanical phenomena in FSW means that this thermal effect can affect the weld mechanical properties. In this work, welds are observed by thermal camera and the effect of secondary heating is seen in the thermal data and the computational fluid dynamics (CFD) model contours. The shank temperature is observed to increase throughout the weld. A similar problem is observed by Kou *et al.* in autogenous gas tungsten arc welding of small-diameter Al-6061 pipe [**2**]. The authors conclude that computer model and experiment show a uniform fusion zone girth during seam welding and a continually increasing fusion zone girth under the same conditions in circumferential welds on small-diameter pipe. The authors propose a preprogrammed reduction in weld power during the weld to reduce fusion zone growth during the process. Lee *et al.* used a state-space optimization method of process parameters to successfully maintain weld pool geometry around the circumference of small-diameter Al-6061 pipe [**3**]. Weld pool geometry was maintained but it was noted that the 450°C isotherm continued to expand.

In a butted pipe configuration, the cylindrical work must be rotated about its axis and this presents issues which complicate the ability to maintain a constant contact condition between the work and shoulder. Eccentricity in the rotation of the pipe combined with eccentricity in the circumference of the pipe sections and variations in pipe thickness result in varying height of the work surface at the tool contact location. If this variation is significant, it can be accounted for by several methods.

One such method is mapping the system eccentricity prior to welding by touching the tool to the work surface at various locations around the circumference. A mapped height path can then be followed during welding [**9**]. Additionally, process force feedback control can be used to compensate for system eccentricity by adjusting vertical tool position or weld parameters based on axial force, torque, or both [**13–16**]. These two methods are used by Lammlein [**17**] for controlling contact condition using the present experimental setup applied to butted hemispheres of similar size.

In the present experiment it was desired to observe the native force oscillations present in a pipe FSW setup of this type without the compensatory influences of in-process contact control and to assess the significance of various pipe FSW issues. By forgoing contact control, the complications inherent to this welding geometry could be observed and techniques could be better developed to compensate for them. In the current experiment, techniques were employed which reduced contact condition variation around the circumference of the pipes to the extent that high-quality welds were reliably produced without the aid of in-process control methods like those described previously. The extent

Downloaded from pib.sagepub.com at VANDERBILT UNIV LIBRARY on February 20, 2012

to which the issues present in FSW on pipe could be managed without process control methods was thus determined. The techniques mentioned enable a more robust FSW process on pipe and are discussed in section 4.

In this work an expandable inner mandrel is used to support and locate the pipe sections during welding. A photo of this setup is shown in Fig. 4. Screws force an interior plug with an outer-diameter taper into the ring anvil which has an inner-diameter taper. A gap cut in the ring anvil allows the ring (or C-shape) to expand against the interior of the pipe sections. An expandable mandrel, as opposed to a press-fit or interference-fit mandrel, allows for insertion and removal of the mandrel without damage to the interior of the pipe. Additionally, this mandrel type can be adjusted to exert the desired degree of support to the interior of the pipe. It was found that a tight inner mandrel both prevented the expulsion or distortion of work material at the root of the weld and more significantly, forced the pipe sections into a more uniformly circular shape. When the pipe sections are forced against one another by the clamping system and the inner mandrel is expanded, the inner circumferences of the two pipe sections are forced to mate and the outer circumferences are mated within the tolerance of the pipe wall thickness. This is important because pipe sections will not be perfectly cylindrical and allowing a greater error tolerance reduces costs and setup time. The precise nature of this clamping methodology readies the pipe sections for the FSW process.

3 WELD TESTS

Full-penetration welds of 4.2" (107 mm) diameter, 0.2" (5.1 mm) thickness butted aluminium alloy (6061-T6) pipe sections were made with two 5/8" (15.9 mm) diameter scrolled shoulder, 0.18" length, threaded probe tools of differing probe diameter. Parameters for a 3/16" (4.8 mm) probe diameter tool were determined based on the superficial appearance, lateral macrosection appearance, and tensile strength of preliminary test welds. Adjustments to all aspects of the setup were then made with emphasis on improving tensile strength. A matrix of welds were then performed with the 3/16" (4.8 mm) probe diameter tool. Process forces were recorded along with the tool shank temperature using a thermal camera. Tensile tests and macrosections were then performed. Based on these results, a second matrix of welds was performed with a 0.236" (6.0 mm) diameter tool. A CFD Fluent model was created for each geometry to complement the experimental results and establish a numerical basis for estimating axial force [**18**, **19**].

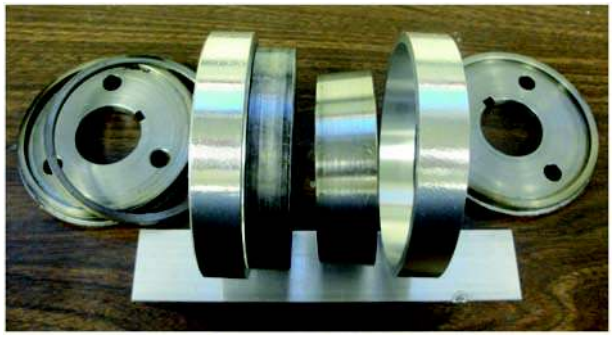

Fig. 4 The expandable mandrel consists of slotted end caps which mate with the keyed axle of the rotary apparatus, a ring anvil with an expansion gap and inner taper, a spacer for centring the anvil, an expansion plug with an outer taper, and bolts (not pictured) to expand the mandrel by pulling the plug towards an end cap and into the taper of the anvil

4 WELD RESULTS AND DISCUSSION

The tensile strengths of the experimental welds are presented in Fig. 5. The ultimate tensile strength (UTS) is plotted as a percentage of the parent UTS. Because of the large number of tested parameters, each data point represents the strength of a single tested tensile coupon. The parent strength (314.6 MPa) was determined by averaging five samples. Generally, the results show an increase in weld strength with increasing traverse rate and rotation rate. This trend holds for all welds with the exception of several at the fastest parameter settings, where increasing speed results in weaker welds. The strength appears to be largely independent of which probe diameter was used. In addition to reduced strength, weld appearance was inconsistent and of reduced quality for the 1400 rpm by 13.1 ipm and 1600 by 17.0 ipm cases. The reduced weld appearance quality experienced at these high traverse rate settings limited the range of tested parameters. Specially designed clamps were used to hold the pipe section tensile coupons.

The axial force was recorded for welds done with the 6-mm-diameter probe tool via strain gauges mounted to the cast-iron spindle head of the welding machine. A finite element analysis (FEA) model of the spindle head was used to determine strain gauge locations which maximized the influence of axial force and minimized the influence of in-plane (x- and y-direction) forces on the strain gauge array

Downloaded from pib.sagepub.com at VANDERBILT UNIV LIBRARY on February 20, 2012

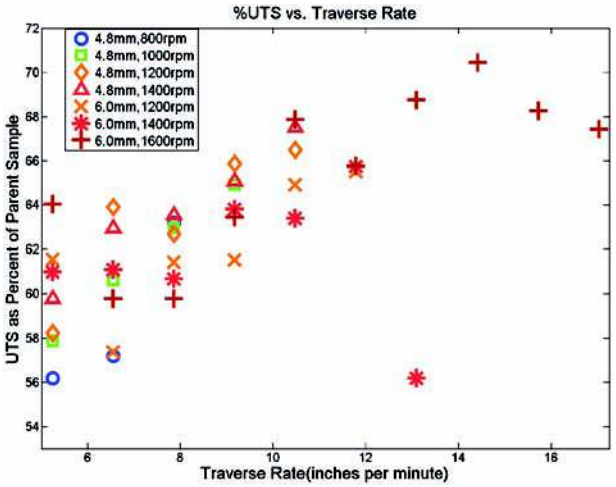

Fig. 5 Ultimate tensile strength (UTS) as a percentage of the parent material UTS versus traverse rate for full-penetration butted pipe welds made with 5/8" diameter, scrolled shoulder and 0.18'' length, threaded probe tools. Data are shown for both the 3/16"(4.8 mm) diameter probe tool and the 0.236"(6 mm) diameter probe tool used in the experiment. Weld tensile strength is observed to increase with increasing process rates with the exception of the extreme cases

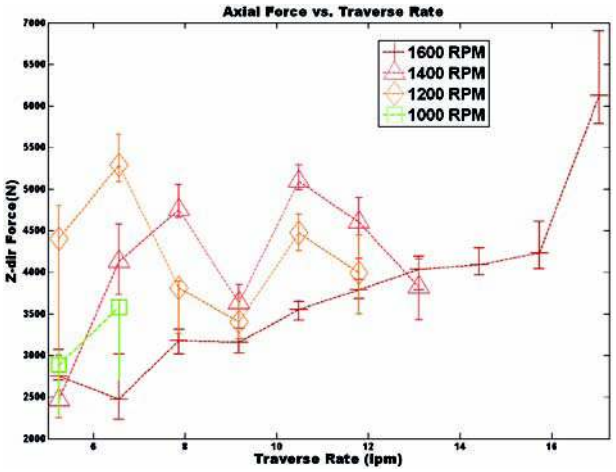

Fig. 6 Experimental axial forces plotted with traverse rate for butted pipe welds made with a 5/8" diameter scrolled shoulder and 6 mm (0.236") diameter threaded probe tool

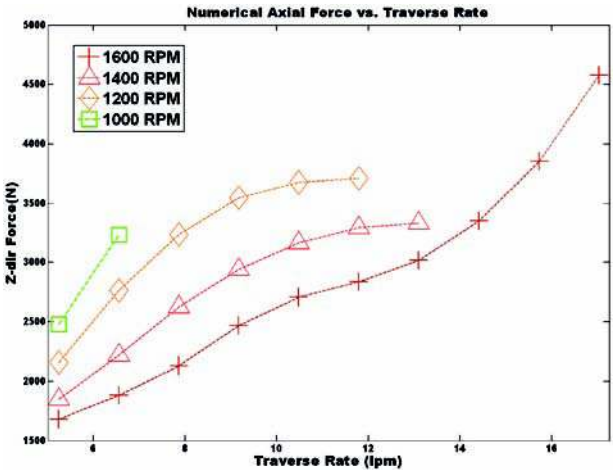

Fig. 7 CFD model axial forces plotted with traverse rate for butted pipe welds made with a 5/8" diameter scrolled shoulder and 6 mm (0.236") diameter threaded probe tool

output. The strain gauge setup was calibrated using a load cell and it was determined that output mapped directly to axial force with negligible cross-influence from in-plane forces. Figure 6 plots the average axial force during the steady-state portion of the weld against traverse rate, for welds made with the scrolled shoulder and 6-mm-diameter threaded probe tool. Figure 6 shows axial force generally increasing with traverse rate. Additionally, forces are more often reduced with increasing rotation rate; however, this association is very loose over the parameter range tested. The highest average axial force occurred at a parameter setting of 1600 rpm and 17.0 ipm. This parameter setting should be considered as on the edge, or outside of, the parameter window which defines acceptable welds, as ideal surface appearance could not be maintained throughout the weld, particularly in the initial portion of the weld where the weld temperature was the lowest. The abrupt jump in axial force at this setting indicates both a lack of plastization and that additional heating is needed to prevent a breakdown of the FSW process.

CFD models have been used with some success to predict the expected axial force encountered during the FSW process based on work material, tool and work geometry, and process parameters [**20**]. Figure 7 shows corresponding axial force values obtained from the Fluent CFD models presented later. The numerical results provide a reasonable estimate of the axial force values seen during the experiment.

Efforts were made to ensure that following proper depth and seating of the tool shoulder at the weld initiation site, forces would subsequently fluctuate within an acceptable range during the weld traverse. Figure 8 shows the axial force history of a selected experimental weld. Keeping force fluctuations within an acceptable range (approximately ± 5 per cent of the weld's mean axial force) was done by means of several techniques. The robustness of these techniques was demonstrated by performing the

Downloaded from pib.sagepub.com at VANDERBILT UNIV LIBRARY on February 20, 2012

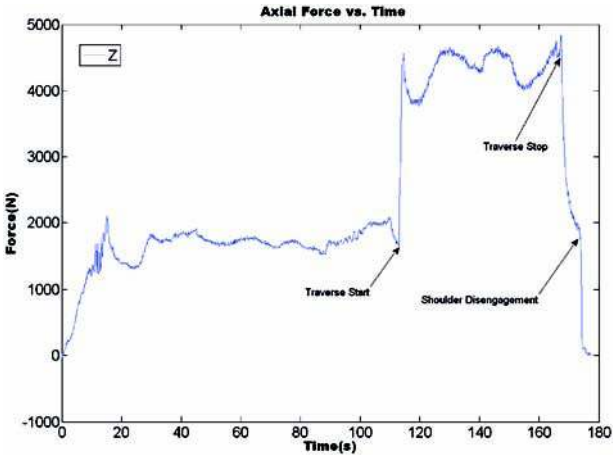

Fig. 8 Axial force history recorded via a calibrated strain gauge array mounted to the spindle head for a weld performed with a 6 mm (0.236") diameter, threaded probe tool at 1600 rpm and 15.7 ipm. Efforts were taken to ensure forces fluctuated within an acceptable range during the welding process

Fig. 9 The 5/8" (15.9 mm) diameter scrolled shoulder, 3/16" (4.8 mm) probe diameter tool used in this experiment. The scrolled shoulder feature increased tolerance to variation in contact condition and improved weld appearance

experiment without the aid of a control algorithm which made in-process vertical adjustments to the system. It is thus demonstrated that these techniques improve the consistency and quality of FSW joints on small-diameter pipe and that the inclusion of one or more of these techniques in addition to a force control scheme would improve process reliability in manufacturing.

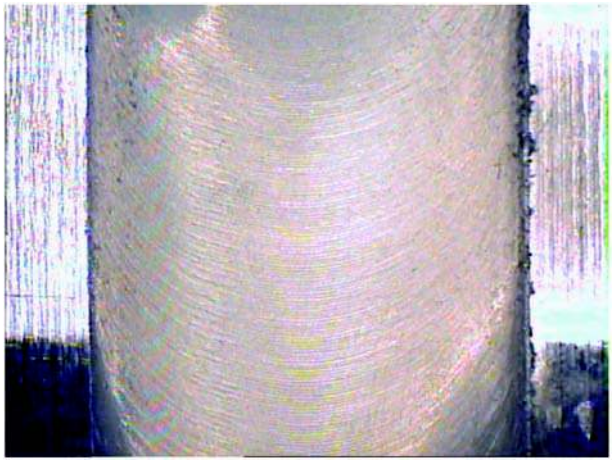

Fig. 10 The superficial appearance of a typical welded pipe specimen (close-up)

The parent pipe sections were machined from their received condition on their inner diameter and outer diameter. After this preprocessing, the wall thickness varied from the approximate thickness of 0.19" by a maximum of 0.005". This tolerance limit was maintained on each pipe section, and between each pipe section, ensuring near-uniform thickness around the circumference of each section and well matched wall thicknesses between pipe sections.

The use of the expanding mandrel, described earlier, forced pipe sections into a more perfect circular shape and aligned the inner diameter of the pipe sections. Together, a fine wall thickness tolerance and a tightly adjusted expanding inner mandrel served to align the joint in the geometric configuration most favourable to joining by FSW. With the use of force control and an expanding mandrel it would be possible to allow a greater wall thickness tolerance and the preprocessing step could be eliminated from the welding procedure [**21**].

The shoulder of both of the tools used in the experiment used a scroll to force material inward from the edge of the shoulder during welding as the tool rotates. The scrolled shoulder is shown in Fig. 9. This feature increased the tolerance of the tool to tool-work contact variations. Figures 10 and 11 show the superficial appearance of the welds. Preliminary welds performed with an unfeatured shoulder tool showed consistent poor surface quality, producing either surface void defects or flash (material expulsion). It proved to be very difficult to produce superficially acceptable welds without a tool with shoulder features.

Downloaded from pib.sagepub.com at VANDERBILT UNIV LIBRARY on February 20, 2012

Finally, the tool was offset 6 mm ahead of the geometric centre of the work along the traverse direction. This created a ploughing effect which reduced tolerance to vertical positioning error. This offset was arrived via experimental trial. It was found that positioning the tool directly over the high point of the pipe (i.e. no offset) resulted in buffeting and an unstable weld condition. Taking these steps meant the experiment could be performed without force control despite the difficulties of system eccentricity and secondary heating present in small-diameter pipe FSW.

The weld macrosections show complete penetration of the weld nugget through the work. Figure 12 shows the appearance of lateral cross-sections of welds made at low rates using the 3/16"-diameter probe (narrow probe) tool. Frames were taken looking down the weld with the retreating side on the left. Weld samples were first mounted, then sanded over silicon carbide discs at various grits finishing with P1500, polished using 0.5 μm alumina suspension, and finally etched by 1 minute bath in Keller's reagent. Figure 13 shows lateral views of remaining welds made using the narrow probe tool. Increasing the width of the probe predictably increases the width of the weld nugget.

Figures 14 to 17 show the lateral macrosections of welds made using the 6-mm-diameter probe (wide probe) tool. These figures show welds performed over the parameter range of 5.2–17 ipm, and 1200–1600 rpm. Figure 18 presents a magnified view of a selected macrosection.

A FLIR thermal camera was used to make thermal videos of the full weld cycle. The camera was calibrated to the emissivity of the tool shank. The curved outer surface of the aluminium pipe sections were too reflective to give reliable emissivity calibration, thus the tool shank was used. The shank temperature was shown to decrease predictably with increasing traverse rate in the experimental data obtained via thermal camera. Higher rotation rates generally resulted in higher temperatures but this relationship was not as consistent in the data. This is because, unlike traverse rate, rotation rate has only a minor influence on temperature in FSW and one which is not consistent and direct in nature over the complete range of traverse rates and welding conditions. The data showed the wide-probe welds to be slightly hotter than the narrow-probe welds. The experimental shank temperature agrees closely with the CFD model results at the modelled parameter (1000 rpm, 5.2 ipm) for both geometry cases. The thermal data from this experiment is presented fully in [**17**].

Figure 19 shows the typical temperature history of the tool shank surface during welding. Temperature on the tool shank surface increases gradually as the probe is plunged into the material and then more

Fig. 11 The superficial appearance of several pipes welded in the experiment

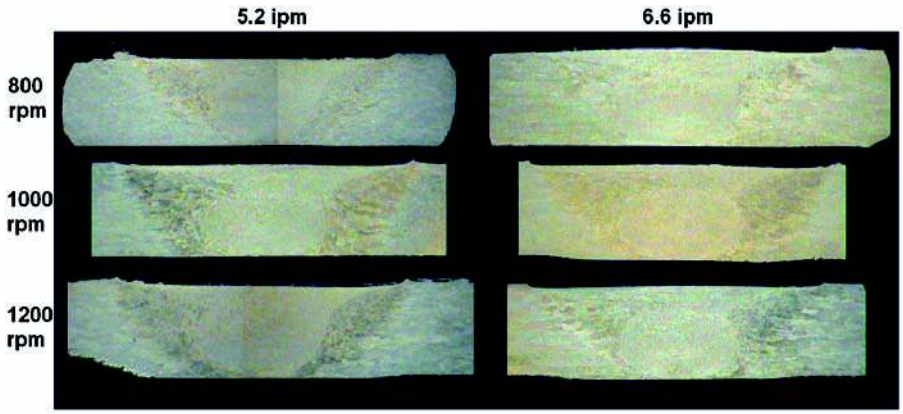

Fig. 12 Lateral macrosection view of welds made at 5.2 and 6.6 ipm using a 5/8"-diameter scrolled shoulder, 3/16"-diameter threaded probe tool. Two of the weld images presented above were made by composition of two photos due to an equipment issue

Downloaded from pib.sagepub.com at VANDERBILT UNIV LIBRARY on February 20, 2012

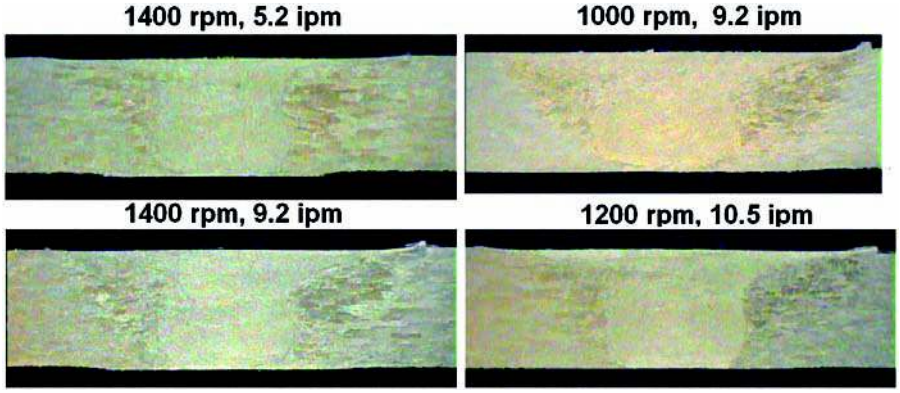

Fig. 13 Macrosections of selected welds made with the narrow probe tool

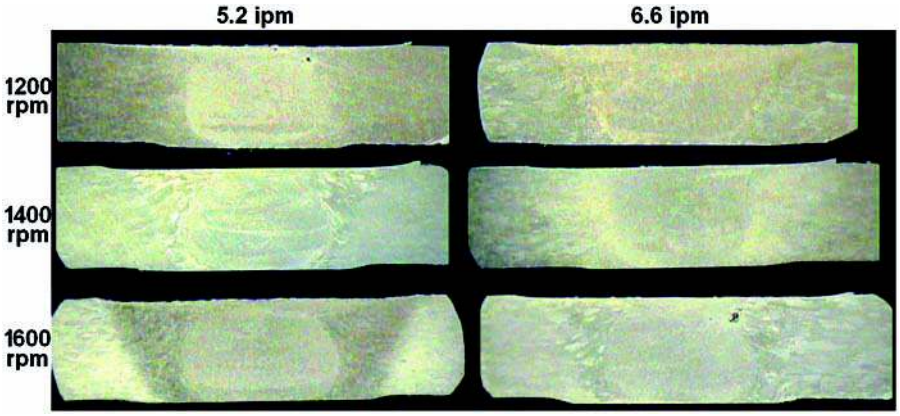

Fig. 14 Lateral macrosection view of welds made at 5.2 and 6.6 ipm using a 5/8″-diameter scrolled shoulder, 0.236"-(6 mm)-diameter threaded probe tool

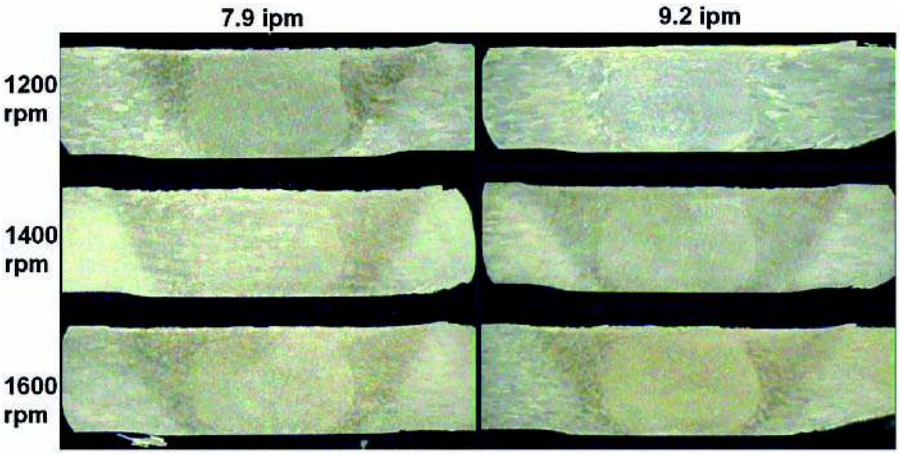

Fig. 15 Macrosections of welds made at 7.9 and 9.2 ipm with the wide probe tool

rapidly as the shoulder contact condition is established. When the shoulder is at the desired position and the traverse is triggered, the temperature increases less rapidly. The issue of secondary heating can be seen during the weld proper in the presented temperature charts. The tool must pass over the weld initiation site, which has been previously subjected to the weld thermal environment, to complete a full

Downloaded from pib.sagepub.com at VANDERBILT UNIV LIBRARY on February 20, 2012

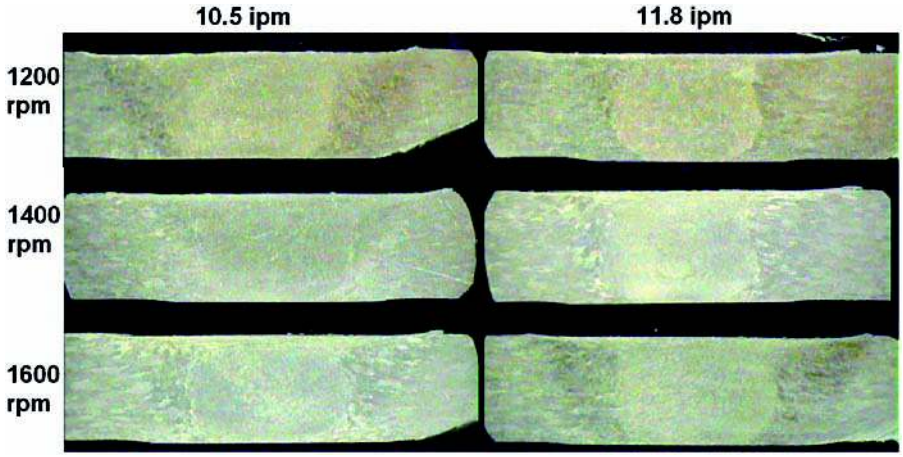

Fig. 16 Macrosections of welds made at 10.5 and 11.8 ipm with the wide probe tool

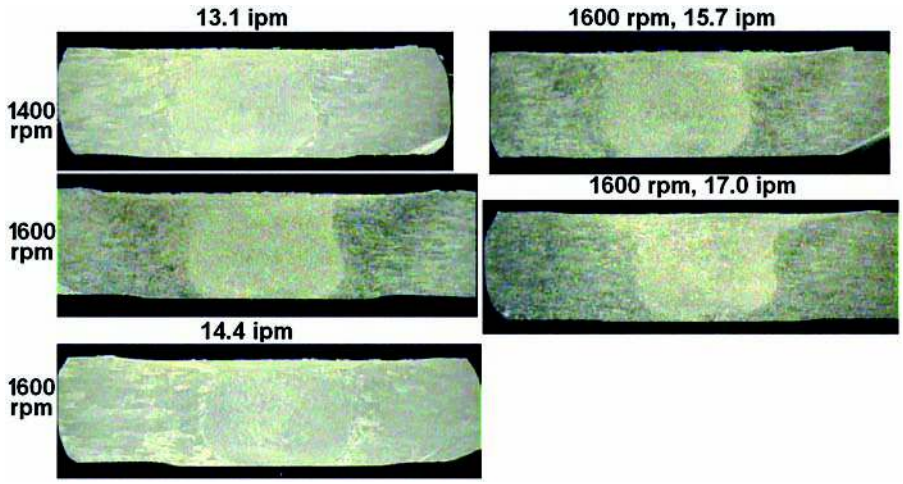

Fig. 17 Macrosections of selected welds made with the wide probe tool

circumferential weld. A steady-state temperature is never reached and temperature increases throughout the weld cycle. In the presented experiment, this climb in temperature did not adversely affect weld quality. However, the temperature increase over the circumference of the weld is significant in small-diameter pipes and could affect weld quality under other conditions.

Fusion welding experiments performed on this material and geometry demonstrated that process parameter adjustment was required around the circumference of the weld to maintain acceptable weld quality throughout [**2, 3**]. Heat input had to be reduced continually to avoid significant and undesirable expansion of the weldpool. It was shown in this study that the reduced welding temperature of the FSW interface minimized this problem and acceptable welds could be produced over a range of parameters. Although a steady rise in temperature was observed, it was not sufficient to require any reduction in weld power during the weld.

During welding of butted plates a similar problem can be encountered when the tool nears the end of the plate and the edge of the plate presents a barrier for heat conduction. This situation near the end of a weld on butted plates is less severe, yet still presents a problem under certain conditions that must be addressed.

5 MODELLING

A numerical model was created for both tool geometries using Ansys Fluent software [**22**]. Fluent is an Eulerian, finite-volume CFD program. The mesh geometries for each tool were created in the preprocessing program, Ansys Gambit [**23**]. The

Downloaded from pib.sagepub.com at VANDERBILT UNIV LIBRARY on February 20, 2012

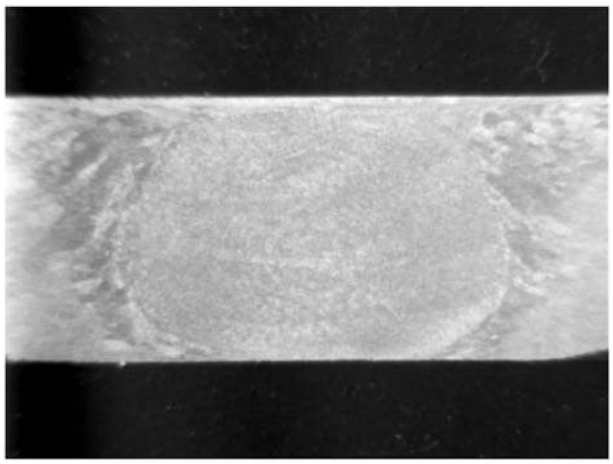

Fig. 18 Zoom view of a macro taken from a full penetration butted pipe weld (1400 rpm, 5.2 ipm). The experimental tools had a 5/8" -diameter, scrolled shoulder and 0.18" -length threaded probe. The wide (0.236" diameter) probe tool created this weld

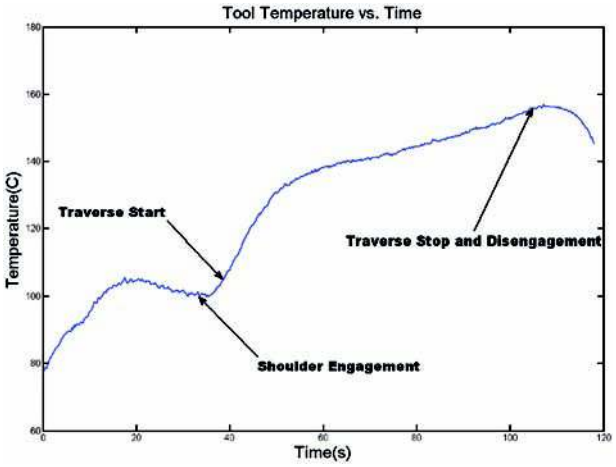

Fig. 19 A chart showing the tool shank thermal history over the course of a selected weld from the experiment. These data were typical of weld thermal data taken during the experiment in that temperature continued to rise throughout the weld

narrow-probe geometry contained 221 887 tetrahedral cells and 465 690 triangular faces, and the wide probe geometry contained 224 689 cells and 471 146 faces. The meshes are fine at the interface. A growth rate was established from the interface, creating tool and material volumes which are increasingly coarse with distance from the interface. The mesh is finest in the work near the interface because temperature and velocity gradients are highest in the vicinity of

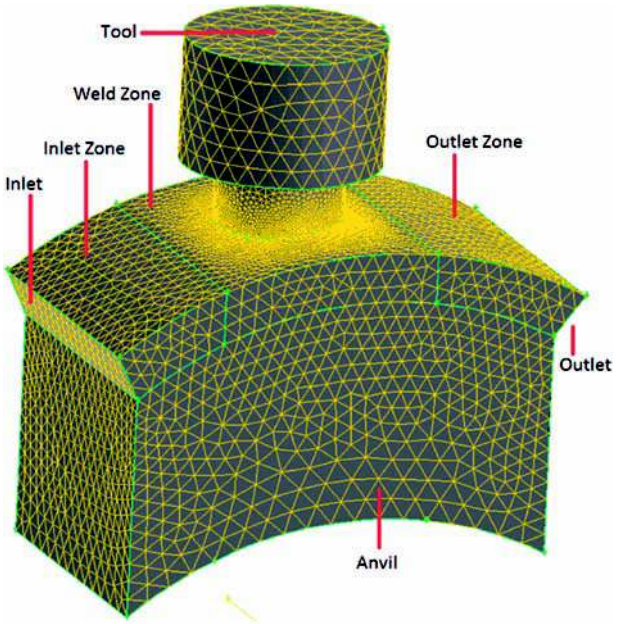

Fig. 20 Computer model geometry created in the Gambit preprocessor showing the inlet, outlet, and model zones

the tool. Figure 20 shows the mesh refinement and geometry. Figure 21 shows the mesh over the tool geometry, created in gambit. The meshes for both cases were then exported and loaded in Fluent.

The implicit formulation was used in Fluent with the laminar viscosity setting. The Presto pressure solver for highly rotating flows was selected due to the relatively high rotation rate with respect to traverse rate. The weld material viscosity function was set by user-defined function and defined using the Carreau viscosity model [**24, 25**]

$$\mu = \mu_\infty + (\mu_0 - \mu_\infty) \left\{1 + \left[\dot{\gamma}\lambda \exp\left(T_0/T\right)\right]^2\right\}^{(n-1)/2} \quad (1)$$

where μ_∞ is the infinite shear viscosity, μ_0 is the zero shear viscosity, $\dot{\gamma}$ is the local shear strain-rate, λ is the time constant, T_0 is the reference temperature, T is the local temperature, and n is the power law index. In the weld zone (see Fig. 20), Carreau constants derived from analytical experiments in Al-6061-T6 were taken (μ_∞=0, μ_0=1-e8 Pa·s, λ=10, n=1, T_0=300 K) [**26**]. For the inlet and outlet zones, a reduced μ_0 of 100 Pa·s was used to aid in solution convergence as flow was not critical in these regions. The total heat input at the interface was determined using the heat generation equation formulated by Schmidt and Hattel [**27**].

Downloaded from pib.sagepub.com at VANDERBILT UNIV LIBRARY on February 20, 2012

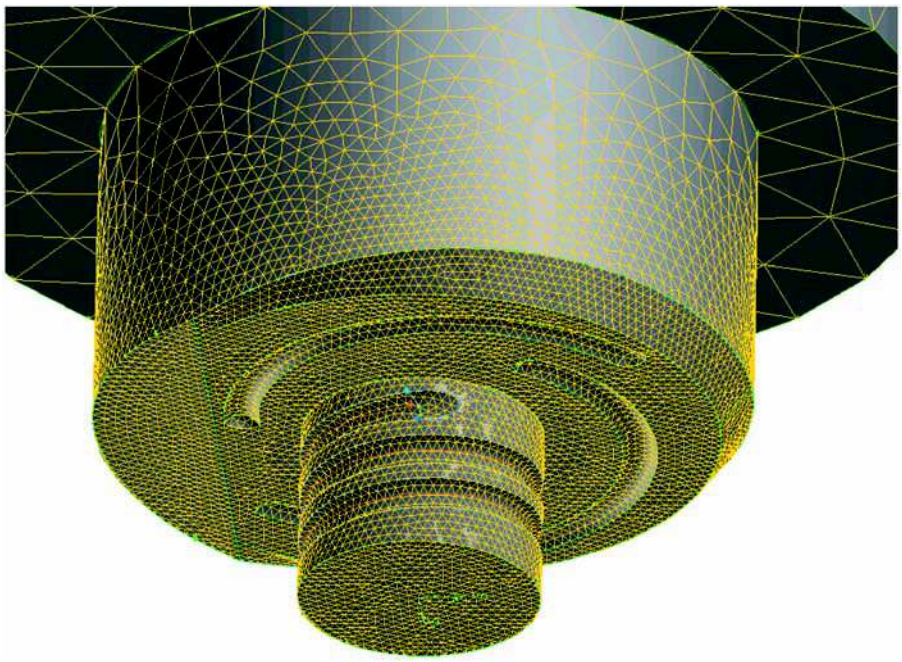

Fig. 21 A close-up view of mesh refinement on the tool face. The featured shoulder and threaded probe can be seen. The mesh was finest at the interface

Schmidt's analytical equation for heat generation approximates the heat generated by the tool based on a sliding contact condition at the interface

$$\mathrm{Q} = \tau_{\mathrm{contact}}\omega \mathrm{Ad} \quad \text{where} \quad \tau_{contact} = \mu \mathrm{P} \tag{2}$$

where Q is heat generated by area A, whose centroid is distance d from the axis of rotation; and τ_{contact} is the contact shear stress, μ is the frictional coefficient, P is the contact pressure, ω is the radial velocity of the tool. For a simple tool with a cylindrical probe the equation becomes

$$\mathrm{Q}_{\mathrm{total}} = \frac{2}{3}\pi\tau_{\mathrm{contact}}\omega\left(\mathrm{R}^3 + 3\mathrm{r}^2\mathrm{h}\right) \tag{3}$$

where R is the radius of the shoulder, r is the radius of the probe, and h is the height of the probe. For the present case the equation must be slightly modified to account for the portion of the shoulder not in contact with the work. This portion of the shoulder is a circular section on the shoulder defined by an inclusive angle of approximately 100°. The area of this non-contact, circular section is calculated by

$$A_{\mathrm{nc}} = \left(\frac{1}{2}\right)R^2[\theta - \sin(\theta)] = \left(\frac{1}{2}\right)\left(\frac{5}{16}''\right)^2[1.745\ \mathrm{rad} - \sin(1.745\ \mathrm{rad})] = 0.037\mathrm{in} = 2.40e-5\ \mathrm{m}^2 \tag{4}$$

where R is the shoulder radius in inches, and θ is the inclusive angle which defines the circular section (100°), in radians. The centroid of this non-contact area is located a distance, D_{nc}, from the tool axis of rotation

$$D_{nc} = \frac{4R\sin(\theta/2)^3}{[3\{\theta - \sin(\theta)\}]} = \frac{4\left(\frac{5}{16}''\right)\left(\frac{1.745rad}{2}\right)^3}{[3\{1.745rad - \sin(1.745rad)\}]} = 0.246'' = 0.0063\ \mathrm{m} \tag{5}$$

where R is the shoulder radius, in inches, and theta is the angle which defines the circular section, in radians. The contact pressure, P, can be calculated by dividing the axial force by the horizontal tool area

$$P = \frac{F_{\mathrm{axial}}}{A_{\mathrm{horiz}}} = \frac{F_{\mathrm{axial}}}{\pi R^2 - A_{\mathrm{nc}}} \tag{6}$$

Using the experimental axial force for the 1000 rpm, 5.2 ipm parameter, the setting contact pressure, P, can be calculated for the width probe and narrow probe tools. Axial force readings were not taken during the narrow probe welds so the value obtained for the wide probe will be used for both cases. The calculated contact pressure for both experimental tools at the 1000 r/min, 5.2 ipm setting is

$$P_{1000,5.2} = \frac{F_{\mathrm{axial}}}{\pi R^2 - A_{\mathrm{nc}}} = \frac{2880.5\ \mathrm{N}}{\pi([0.0079\ \mathrm{m})]^2 - (2.40\,e-5\ \mathrm{m}^2)} = 1.66\,\mathrm{e}-7\ \mathrm{Pa} \tag{7}$$

For the experimental contact condition the general Schmidt equation becomes

$$Q_{\mathrm{tool}} = \mu \mathrm{P}\omega\left[\frac{2}{3}\pi\left(\mathrm{R}^3 + 3\mathrm{r}^2\,\mathrm{h}\right) - A_{\mathrm{nc}}D_{\mathrm{nc}}\right] \tag{8}$$

Downloaded from pib.sagepub.com at VANDERBILT UNIV LIBRARY on February 20, 2012

For the 1000 r/min, 5.2 ipm setting and the narrow probe tool using an assumed value of 0.7 for the frictional coefficient, the heat generated by the narrow probe tool, Q_n, *is*

$$Q_n = (0.7)(1.66e-7)(104.72)\left[\frac{2}{3}\pi((0.079)^3 - 3(.0024)^2.0046) - (2.4e-5).0063\right] = 1,287\,\text{watts} \quad (9)$$

where 0.7 is the friction coefficient, 1.66e-7 Pa is the contact pressure, 1000 rpm (104.72 rad/s) is the tool rotation rate, 5/16" (0.0079 m) is shoulder radius, 3/32" (0.0024 m) is the probe radius, 0.18" (0.004 m) is the probe height, 0.037 in^2 (2.4e-5 m^2) is the non-contact area, and 0.246" (0.0063 m) is the non-contact centroid distance. For the wide probe tool this equation gives

$$Q_n = (0.7)(1.66e-7)(104.72)\left[\frac{2}{3}\pi((0.079)^3 - 3(.003)^2.0046) - (2.4e-5).0063\right] = 1,403\,\text{watts} \quad (10)$$

where only the radius of the wide probe tool, 0.118'' (0.003 m), is substituted from the previous calculation. The slightly increased surface area of the probe and the slightly higher relative velocity of the probe wall result in higher heat input for the fat probe tool at identical parameters.

Although torque values for this experiment were not obtained, a secondary estimate of weld thermal input can be obtained via the weld power method by using a torque value taken from a similar experiment under similar conditions. A value of 10.56 N·m is taken from an experiment performed on butted spheres of identical (0.2r) thickness using the same rotary welding apparatus. The tool shoulder from this case was of the same 5/8r diameter but was cupped in geometry to mate with the spherical work. Like the present case this value was taken over a 1000 rpm weld, however, the lowest traverse rate recorded during the analogue spherical experiment at the 1000 rpm rotation rate was 7.8 ipm, so an extrapolated value is taken. The probe was 3/16r diameter and threaded and therefore will be compared with the 3/16" diameter probe calculation. Using the weld power method where Ω is weld torque [**28**]

$$Q_{\text{n,weldpower}} = \Omega\omega = (10.56\,\text{N}\cdot\text{m})\left(104.7\frac{\text{rad}}{\text{s}}\right) = 1106\,\text{watts} \cong 1287\ \text{watts} \quad (11)$$

An upper-limit weld power can be calculated using an upper-limit weld torque obtained by applying the measured axial load at the very edge of the tool shoulder. For the wide-probe modelled case this yields

$$Q_{\text{w,upperweldpower}} = FR\omega = 2880.5\,\text{N}(0.0079\,\text{m})\left(104.7\frac{\text{rad}}{\text{s}}\right) = 2394\ \text{watts} \quad (12)$$

For the presented models, the Q_n and Q_w heat rate or power values are used for the narrow-probe and wide-probe models respectively. Heat was distributed across the weld interface and input into the work material as defined by a user-defined function which applied heat locally in proportion to the local tool velocity. This results in highest energy input at the edge of the shoulder where the local tool velocity is highest. A second user-defined function was used to impose the temperature on the work side of the interface onto the adjacent interface cells on the tool side of the interface. This formulation resulted in 5.1 per cent of the total weld power entering the tool in the narrow probe case and 6.6 per cent entering the tool in the wide-probe case. The total heat input into cells on both sides of the interface was equal to the values obtained by the Schmidt formula. A rotational velocity of 1000 rpm and traverse speed of 5.2 ipm were used in the presented models of the narrow-probe and wide-probe geometries. Additionally, cases were run for the wide-probe geometry at all parameters used experimentally in order to provide a numerical estimation of axial force for comparison with experiment.

In Fluent, the tool rotational axis is maintained stationary while velocity-inlet-type boundary conditions are used at the inlet and outlet boundaries to establish material flow past the tool, as when traversing. The outlet boundary condition (BC) can be defined as a velocity inlet with negative magnitude because the flow far from the tool in the work is known to be the traverse rate. A pressure outlet or outflow boundary condition at the outlet would not take advantage of this knowledge and would instead force Fluent to arrive at some flow profile. Thermal BCs are defined as 10 W/(m^2·K) for exposed surfaces and 150 W/(m^2·K) for intimate metal-to-metal contact. The rotating and exposed surface of the tool was defined as 50 W/(m^2·K). Additionally, a wall emissivity of 0.2 was applied to exposed aluminium surfaces and 0.5 to exposed steel surfaces.

The FSW environment presents an extreme fluid case for Fluent software. Temperature and velocity gradients are steep in the vicinity of the tool and the tool rotational velocity is high with respect to the

Downloaded from pib.sagepub.com at VANDERBILT UNIV LIBRARY on February 20, 2012

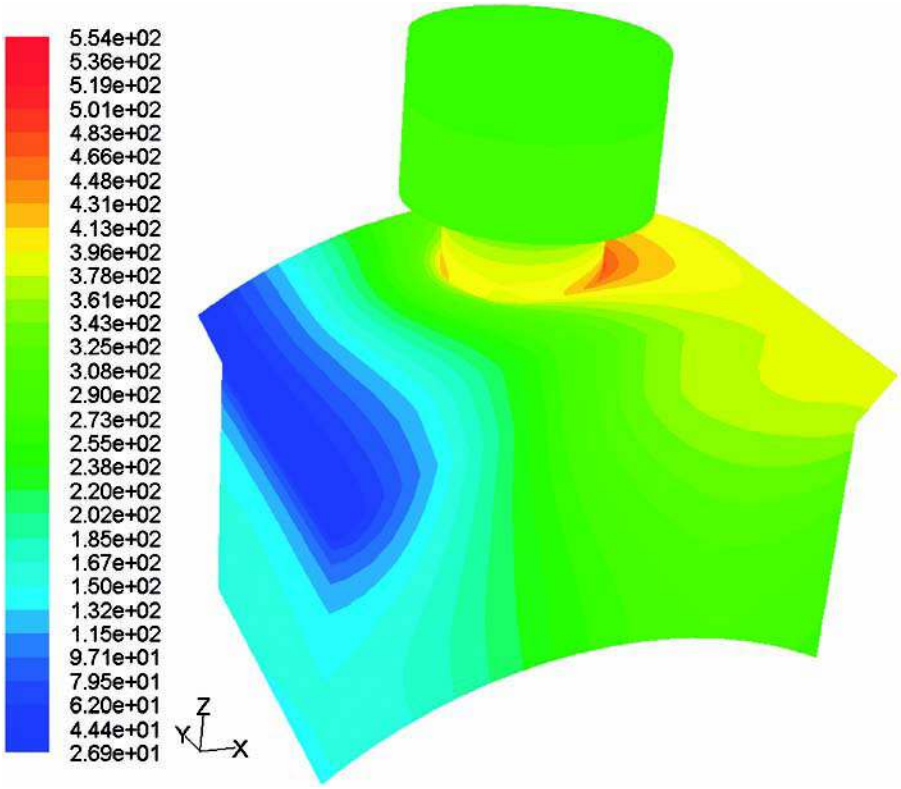

Fig. 22 Modelled temperature contour (C) for the wide 0.236"(6 mm)-diameter probe tool case (Iso view)

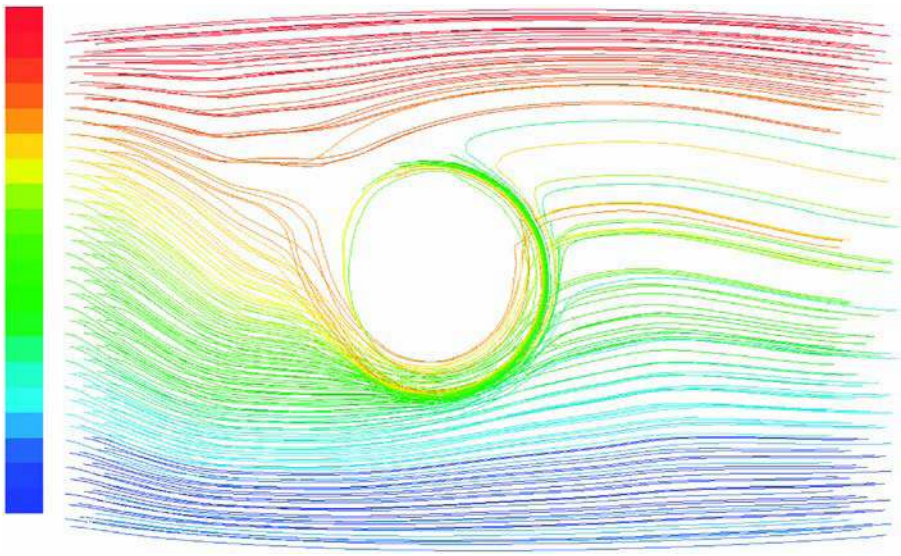

Fig. 23 Model pathlines for the wide-probe tool case (looking from the top, advancing side is red)

traverse speed. Iterating the models starting with the full zero shear viscosity and tool rotational velocity results in divergence errors. In CFD software it is best practice that best guess initial conditions be provided to simplify arrival at a solution. The models presented were initialized using the full experimental traverse speed. From this point, it was found that a solution was best reached in the

Downloaded from pib.sagepub.com at VANDERBILT UNIV LIBRARY on February 20, 2012

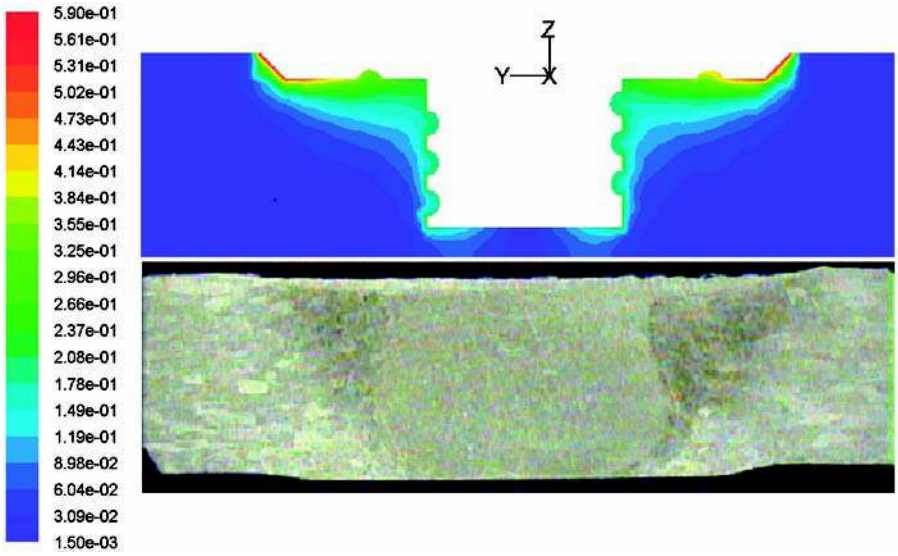

Fig. 24 Lateral contour of velocity magnitude (m/s) compared with experimental lateral macrosection for the wide (6 mm diameter) probe case. The stirred zone (light, centre), thermomechanically affected zone (TMAZ) (dark), and parent material (lightest) can be seen in the macrosection. The model shows significant material stirring in the stirred zone, minimal material stirring in the TMAZ, and no material stirring in the parent material

presented models by successive increases in tool rotational velocity and zero shear viscosity from a small fraction of their desired values to, eventually, their desired values. Using this method, each solution has a good guess solution from which to converge on a subsequent solution using the updated parameters.

Figures 22 to 24 present model contours for the wide-probe case. A contour of temperature, a model pathline flow history, and a figure comparing the lateral contour of velocity magnitude to a lateral macrosection for the wide-probe tool case are presented respectively. The extent of the thermomechanically affected zone (TMAZ) and stirred zone, along with the heat-affected zone, can be seen in the model contours of velocity and temperature respectively. The comparison in Fig. 24 shows the TMAZ and stirred zones determined by the model in comparison to a corresponding experimental macrosection. In this manner the size and shape of these crucial zones can be determined from the model. Additionally, it was shown in Figs 6 and 7 that axial force values can be predicted from the model.

CFD modelling of FSW is well established and understood. It can be used to reliably predict process conditions prior to welding in the manners described above and to make adjustments to the process. An FSW machine is itself expensive and the time required to design and perform an experiment can be significant. CFD modelling of the process is thus justified as a relatively quick, cheap, and reliable tool for process prediction in FSW.

6 CONCLUSIONS

A secondary heating effect was observed due to the tool traversing the weld initiation area twice during the full circumferential welds. Although measured weld temperature increased throughout the weld, the increase was not large enough to necessitate a feedback method for controlling weld temperature (e.g. tool rotation speed adjustment). The authors do however recommend that this process control method be used in manufacturing.

It was shown that a traditional FSW tool geometry could be used on a small-diameter pipe provided that a scrolled shoulder was used and the tool was offset some distance from the centre of the cylindrical work in the direction of traverse as described earlier.

It was demonstrated in this experiment that preprocessing pipe sections to reduce wall thickness variations and applying a stiff inner mandrel resulted in a more robust pipe welding process. The expanding mandrel served to align the inner diameters of the pipe sections and force the sections into a more uniform circular shape.

Using the techniques mentioned, the process can be performed effectively and reliably without the aid of an in-process control method (i.e. force control,

Downloaded from pib.sagepub.com at VANDERBILT UNIV LIBRARY on February 20, 2012

position control). The authors recommend the use of force control in addition to techniques used in the experiment.

Welds presented in the experiment were of high tensile strength and sound internal and superficial appearance. This experiment demonstrated that FSW can be performed on this geometry at a wide range of parameters.

The highest tensile strength was achieved at traverse speed of 15.7 inches per minute and traverse speeds up to 17 inches per minute were tested with good results. At the later speed setting, the tool welds the full circumference of the 4.2″-diameter pipe sections in less than 50 seconds. The ability to weld at high traverse speeds increases the output of an FSW machine and increases the likelihood that the costs of the machine can be justified in a specific manufacturing setting.

CFD models were used to reliably predict the thermal conditions and material flow during FSW of the present geometry. It was shown that CFD can give a reasonable prediction of the axial forces that should be expected under various FSW conditions. The large startup costs associated with FSW make the predictive capabilities and understanding provided by a CFD model more valuable.

ACKNOWLEDGEMENTS

The authors would like to acknowledge the financial support of the Tennessee Space Grant, NASA, and Los Alamos National Lab. The primary author would like to thank UTSI Tullahoma and Kate Lunsford for use of the macrosectioning facilities and assistance. Additionally the contributions of the skilled machinists Bob Patchin and John Fellenstein are acknowledged.

© IMechE, 2011

REFERENCES

1 **Thomas, W. M., Nicholas, E. D.,** and **Needham, J. C.** *Friction stir butt welding.*, 1991 (PCT/GB92/02203 International Patent Application).
2 **Kou, S.** and **Le, Y.** Heat Flow during the autogenous GTA welding of pipes. *Metall. Trans. A.*, 1984, **15**, 1171.
3 **Na, S. J.** and **Lee, H. J.** A study on parameter optimization in the circumferential GTA welding of aluminium pipes using a semi-analytical. *J. Mater. Process. Technol.*, 1996, **57**, 95–102.
4 **Newell, W. F., Sperko, W. J.,** and **Mannings, D C.** *D10 Committee on pipe and tube welding, A.* 2009, p.32.
5 **Feng, Z., Steel, R., Packer, S.,** and **David, S.** *Friction stir welding of API grade X65 steel pipes* (Oak Ridge National Laboratory, U.S. Department of Energy).
6 **Defalco, J.** and **Steel, R.** Friction stir process now welds steel pipe. *The Welding J.*, 2009, **88**, 44–48.
7 **Packer, S. M.** and **Matsunaga, M.** Friction stir welding equipment and method for joining X65 pipe. In Proceedings of the 14th International Offshore and Polar Engineering Conference, Toulon, France, 2004, 55–60.
8 **Fairchild, D., Kumar, A.,** and **Ford, S.** Research concerning the friction stir welding of linepipe steels. In Proceedings of the Trends in Welding Research Conference, Pine Mountain, GA, 2009, 371-380.
9 **Lammlein, D. H., Longhurst, W. H., DeLapp, D. R., Fleming, P. A., Strauss, A. M.,** and **Cook, G. E.** The friction stir welding of hemispheres – a technique for manufacturing hollow spheres. *J. Adv. Manuf.* submitted for publication 5 August, 2010.
10 **Ding, J.** and **Oelgoetz, P.** *The hydraulic controlled auto-adjustable pin tool for friction stir.*, 1996 (NASA)U.S. Patent #5893507.
11 **Trapp, T., Fisher, J.,** and **Bernath, J.** *Method of friction stir welding and retractable shoulderless variable penetration friction stir welding tool for same.*, 2007 (Edison Welding Institute (ESI))U.S. Patent #7234626.
12 **Takeshita, R.** and **Hibbard, T.** *Friction plug welding.* 1998, U.S. Patent #5718366.
13 **Longhurst, W. R., Strauss, A. M., Cook, G. E., Cox, C. D., Hendricks, C. E.,** and **Gibson, B. T.** Investigation of force controlled friction stir welding for manufacturing and automation. *Proc. Inst. Mech. Eng., Part B: J. Engng Manuf.,* 2010, **224**, 937–949. DOI: 10.1243/09544054JEM1709
14 **Longhurst, W. R., Strauss, A. M.,** and **Cook, G. E.** Identification of the key enablers for force control of friction stir welding. *ASME J. Manuf. Sci. Engng* 2009.
15 **Longhurst, W. R., Strauss, A. M.,** and **Cook, G. E.** Enabling automation of friction stir welding: the modulation of weld seam input energy by traverse speed force control. *ASME J. Dynam. Syst. Meas. Control,* 2009, **132**, No 4.
16 **Longhurst, W. R., Strauss, A. M., Cook, G. E.,** and **Fleming, P. A.** Torque control of friction stir welding for manufacturing and automation. *Int. J. Adv. Manuf. Technol.*, 2010, **51**, 905–913.
17 **Lammlein, D. H.** Friction stir welding of spheres, cylinders, and T-joints. *PhD Dissertation*, 2010 (Vanderbilt University, Nashville, TN).
18 **Lammlein, D. H., DeLapp, D. R., Fleming, P. A., Strauss, A. M.,** and **Cook, G. E.** The application of shoulderless conical tools in friction stir welding: An experimental and theoretical study. *Mater. Design*, 2009, **30**, 4012–4022.
19 **Atharifar, H., Lin, D. C.,** and **Kovacevic, R.** Studying tunnel-like defect in friction stir welding process using computational fluid dynamics. *Mater. Sci. Technol.*, 2007, **3**, 1650–1666.
20 **Atharifar, H., Lin, D. C.,** and **Kovacevic, R.** Numerical and experimental investigations on the loads carried by the tool during friction stir welding. *J. Mater. Engng Performance*, 2009, **18**, 339–350.

Downloaded from pib.sagepub.com at VANDERBILT UNIV LIBRARY on February 20, 2012

21 **Longhurst, W. R.** *Force control in friction stir welding*. PhD Dissertation, Vanderbilt University, Nashville, TN, 2009.
22 **ANSYS Inc.** (Canonsburg, PA), *FLUENT CFD (Software)*. Version 6.2.36.
23 **ANSYS Inc.** (Canonsburg, PA), *GAMBIT (Software)*. Version 2.3.16.
24 **Tanner, R.** *Engineering rheology*, 2000, (Oxford University Press, Oxford).
25 **Bird, R. B., Armstrong, R. C.,** and **Hassager, O.** *Dynamics of polymeric liquids: fluid mechanics,* 2nd edition, vol. 1, pp. 210–211.
26 **Tello, K. E., Gerlich, A. P.,** and **Mendez, P. F.** Constants for hot deformation constitutive. *Sci. Technol. Weld. Join.,* 2010, **15**(3), 260–266.
27 **Schmidt, H., Hattel, J.,** and **Wert, J.** An analytical model for the heat generation in friction stir welding. *Modell. Simul. Mater. Sci. Engng*, 2004, **12**, 143–157.
28 **Pew, J. W., Nelson, T. W.,** and **Sorensen, C. D.** Torque based weld power model for friction stir welding. *Sci. Technol. Weld. Join.*, 2007, **12**(4), 341.

APPENDIX

Notation

A	area, m
h	height of probe, m
P	contact pressure, Pa
Q	heat, W
R	radius of shoulder, m
r	radius of probe, m
T	temperature, K
T_0	reference temperature, K
μ_∞	infinite shear viscosity, Pa·s
$\mu_\mathbf{0}$	infinite shear viscosity, Pa·s
$\dot{\gamma}$	strain-rate, m/(m·s) or s^{-1}
ω	radial velocity, rad/s
μ	frictional coefficient
τ	shear stress, Pa

Downloaded from pib.sagepub.com at VANDERBILT UNIV LIBRARY on February 20, 2012